Hindawi
Complexity
Volume 2019, Article ID 5034025, 15 pages
https://doi.org/10.1155/2019/5034025

Research Article

Some Novel Complex Dynamic Behaviors of a Class of Four-Dimensional Chaotic or Hyperchaotic Systems Based on a Meshless Collocation Method

Du Mingjing[1] **and Yulan Wang**[2]

[1]*Institute of Computer Information Management, Inner Mongolia University of Finance and Economics, Hohhot 010070, China*
[2]*Department of Mathematics, Inner Mongolia University of Technology, Hohhot 010051, China*

Correspondence should be addressed to Yulan Wang; wylnei@163.com

Received 29 May 2019; Revised 15 August 2019; Accepted 10 September 2019; Published 20 October 2019

Guest Editor: Murari Andrea

In the field of complex systems, there is a need for better methods of knowledge discovery due to their nonlinear dynamics. The numerical simulation of chaotic or hyperchaotic system is mainly performed by the fourth-order Runge–Kutta method, and other methods are rarely reported in previous work. A new method, which divides the entire intervals into N equal subintervals based on a meshless collocation method, has been constructed in this paper. Some new complex dynamical behaviors are shown by using this new approach, and the results are in good agreement with those obtained by the fourth-order Runge–Kutta method.

1. Introduction

This paper shows some novel complex dynamical behaviors of a class of four-dimensional chaotic or hyperchaotic systems, and a four-dimensional system (1) is adopted as an example to elucidate the solution process.

We consider the following four-dimensional system:

$$\begin{bmatrix} \frac{dx}{dt} \\ \frac{dy}{dt} \\ \frac{dz}{dt} \\ \frac{dw}{dt} \end{bmatrix} = \begin{bmatrix} a_{11} & a_{12} & a_{13} & a_{14} \\ a_{21} & a_{22} & a_{23} & a_{24} \\ a_{31} & a_{32} & a_{33} & a_{34} \\ a_{41} & a_{42} & a_{43} & a_{44} \end{bmatrix} \begin{bmatrix} x \\ y \\ z \\ w \end{bmatrix} - \begin{bmatrix} 0 \\ a_1 xz \\ a_2 x^2 + a_3 y^2 + a_4 xy \\ 0 \end{bmatrix}, \quad 0 \le t \le T, \tag{1}$$

with the following initial conditions:

$$\begin{aligned} x(0) &= c_1, \\ y(0) &= c_2, \\ z(0) &= c_3, \\ w(0) &= c_4, \end{aligned} \tag{2}$$

where $x, y, z,$ and w are the state variables and $a_{ij}, a_i,$ and c_i are the positive parameters of the system. We assume that the solution of systems (1) and (2) exists and it is unique.

In recent years, some new four-dimensional chaotic or hyperchaotic systems [1–7] are presented. In [1], the authors presented a four-dimensional hyperchaotic system and investigated and analyzed some complex dynamical behaviors such as ultimate boundedness, chaos, and hyperchaos. In [2], the authors reported a four-dimensional dissipative chaotic system, and the coexistence of rich chaotic dynamics in the system was investigated through the Lyapunov spectrum, bifurcation diagram, Poincarė map, frequency spectrum, and attractor plot. In [3], the authors discussed the synchronization between two chaotic dynamical systems of different order using an adaptive control scheme. In [4],

a four-dimensional autonomous system with complex hyperchaotic dynamics was presented, and the complex dynamical behaviors were investigated by dynamical analysis approaches, such as time series, Lyapunov exponent spectra, bifurcation diagram, and phase portraits. In [1–8], the authors used the fourth-order Runge–Kutta method to simulate chaotic or hyperchaotic systems. In this paper, we mainly introduce an improved meshless collocation method to simulate hyperchaotic systems with long-time dynamic behavior.

2. The Meshless Collocation Method

A hyperchaotic system has two or more positive Lyapunov exponents. At least four dimensions for the integer order continuous autonomous system are needed in order to generate a hyperchaotic system. Chaotic sequences of such system are more dependent on the parameters and initial conditions, and their dynamic behaviors are more difficult to predict. Its attractors are more complex than general attractor. Diffusion and confusion can be carried out simultaneously in several dimensional spaces. Therefore, the hyperchaotic system has a distinct advantage over low dimensional chaos, and its high-precision numerical solution is very important.

In this section, we introduce an improved meshless collocation method to solve the four-dimensional chaotic or hyperchaotic system, and the main points are as follows.

We transform system (1) into equation (5) using the meshless collocation method [9]. We construct the following linear iterative format of system (1):

$$\begin{bmatrix} \frac{dx_n}{dt} \\ \frac{dy_n}{dt} \\ \frac{dz_n}{dt} \\ \frac{dw_n}{dt} \end{bmatrix} = \begin{bmatrix} a_{11} & a_{12} & a_{13} & a_{14} \\ a_{21} & a_{22} & a_{23} & a_{24} \\ a_{31} & a_{32} & a_{33} & a_{34} \\ a_{41} & a_{42} & a_{43} & a_{44} \end{bmatrix} \begin{bmatrix} x_n \\ y_n \\ z_n \\ w_n \end{bmatrix} - \begin{bmatrix} 0 \\ a_1 x_{n-1} z_n \\ a_2 x_{n-1} x_n + a_3 y_{n-1} y_n + a_4 x_{n-1} z_n \\ 0 \end{bmatrix}. \tag{3}$$

Using the meshless collocation method, $x_n(t), y_n(t), z_n(t), w_n(t)\,(n = 1, 2, 3, \ldots)$ can be written as [9, 10]

$$\begin{aligned} x_n(t) &= \sum_{j=1}^{M} r_j(t) x_n\left(t_j\right), \\ y_n(t) &= \sum_{j=1}^{M} r_j(t) y_n\left(t_j\right), \\ z_n(t) &= \sum_{j=1}^{M} r_j(t) z_n\left(t_j\right), \\ w_n(t) &= \sum_{j=1}^{M} r_j(t) w_n\left(t_j\right), \end{aligned} \tag{4}$$

where the barycentric interpolation primary function $r_j(t) = (\omega_j/t - t_j)/\sum_{k=1}^{M}(\omega_k/t - t_k)$ and $\omega_j = 1/\prod_{i=1, j\neq k}^{M}(t_i - t_j)$ is the center of gravity interpolation weight.

Inserting (4) into (3) and then letting $t = t_i$, the format (3) can be transformed into the following linear algebraic equations [9, 10]:

$$\begin{bmatrix} D - a_{11}I & -a_{12}I & -a_{13}I & -a_{14}I \\ -a_{21}I & D - a_{22}I & -a_{23}I + a_1\mathrm{diag}\left(x_{n-1}\right) & -a_{24}I \\ -a_{31}I + a_2\mathrm{diag}\left(x_{n-1}\right) & -a_{32}I + a_3\mathrm{diag}\left(y_{n-1}\right) & D - a_{33}I + a_4\mathrm{diag}\left(x_{n-1}\right) & -a_{34}I \\ -a_{41}I & -a_{42}I & -a_{43}I & D - a_{44}I \end{bmatrix} \begin{bmatrix} x_n \\ y_n \\ z_n \\ w_n \end{bmatrix} = \begin{bmatrix} 0 \\ 0 \\ 0 \\ 0 \end{bmatrix}, \tag{5}$$

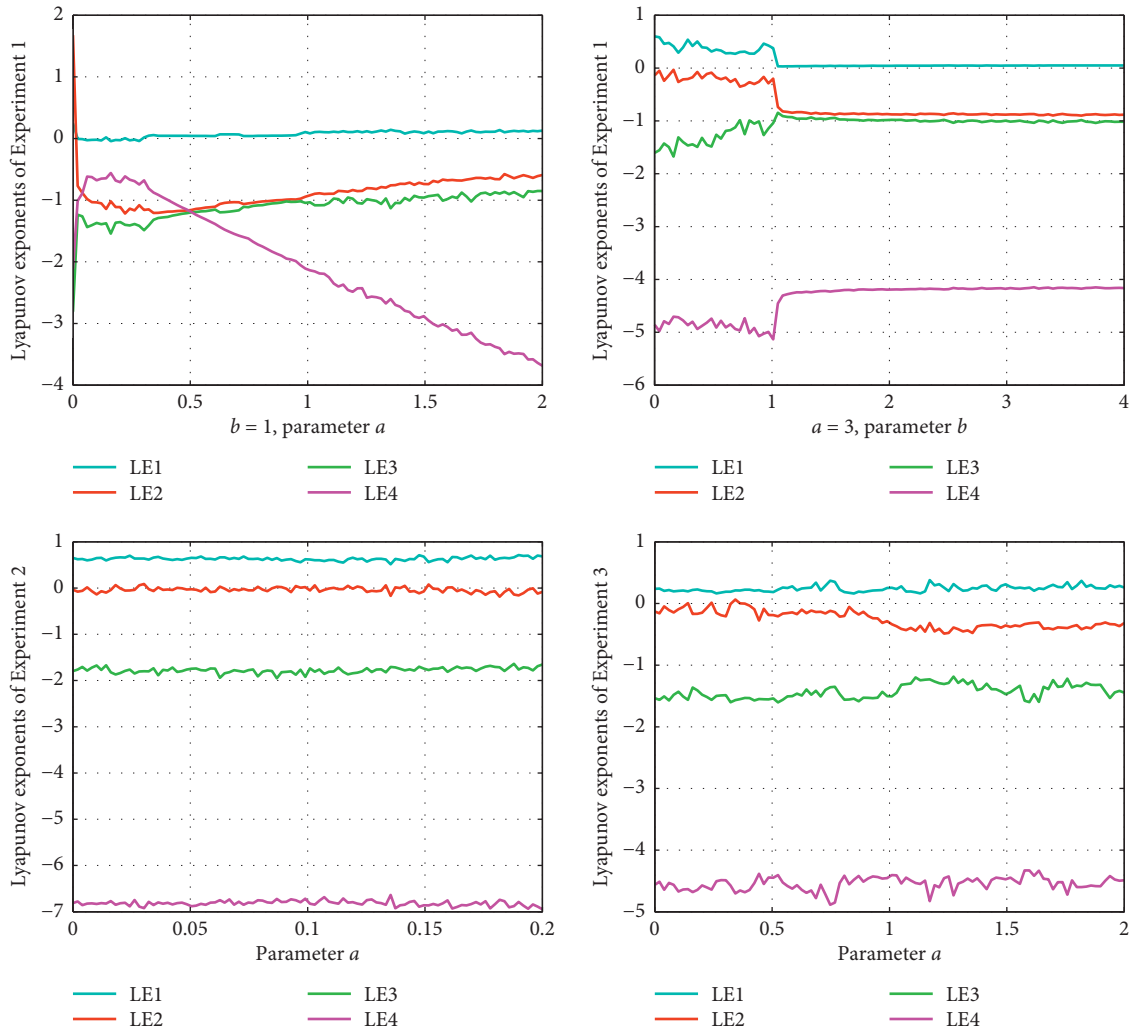

Figure 1: Lyapunov exponents of Experiment 1–3.

where $D = (r_j'(t_i))_{i,j=1,2,\ldots,M}$ is the M-order matrix, I is the M-order unit matrix, and the vector $[x_n, y_n, z_n, w_n] = [x_n(t_1), x_n(t_2), \ldots, x_n(t_M), y_n(t_1), y_n(t_2), \ldots, y_n(t_M), z_n(t_1), \ldots, z_n(t_M), w_n(t_1), \ldots, w_n(t_M)]$.

Schneiaer and Werner [11] introduced the meshless collocation method by using higher-order rational interpolation functions. The barycentric representation of the rational interpolation function possesses various advantages in comparison with other representations such as continued fractions. Baltensperger and Berrut [12] introduced the meshless collocation method for solving general hyperbolic problems and proved its stability and its convergence in weighted norms. Li and Wang [13, 14] presented the algorithm and program of the meshless collocation method and had indicated the meshless collocation method has a high accuracy, good stability, and convergence [15–19]. However, the method cannot apply directly the solving of hyperchaotic system due to great errors. Therefore, an improved mesheless collocation method, which divides the entire intervals $[0, T]$ into N equal subintervals, is constructed in the following section.

We obtain the solution of equation (5) on every intervals $[T_j, T_{j+1}]$.

Dividing the interval $[0, T]$ into N equal subintervals $[T_j, T_{j+1}]$, $j = 0, 1, \ldots, N-1$, letting $\Delta T = T_{j+1} - T_j$ with $T_0 = 0$ and $T_N = T$. On $[T_0, T_1]$, selecting the second kind Chebyshev nodes $t_i = T_1/2\,(1 - \cos(\pi i/M))$, $i = 0, 1, 2, \ldots, M$, and using (4) and the initial conditions (2), we can get

$$\begin{aligned}
\sum_{i=1}^{M} r_i(0) x_n(t_i) &= c_1,\\
\sum_{i=1}^{M} r_i(0) y_n(t_i) &= c_2,\\
\sum_{i=1}^{M} r_i(0) z_n(t_i) &= c_3,\\
\sum_{i=1}^{M} r_i(0) w_n(t_i) &= c_4.
\end{aligned} \tag{6}$$

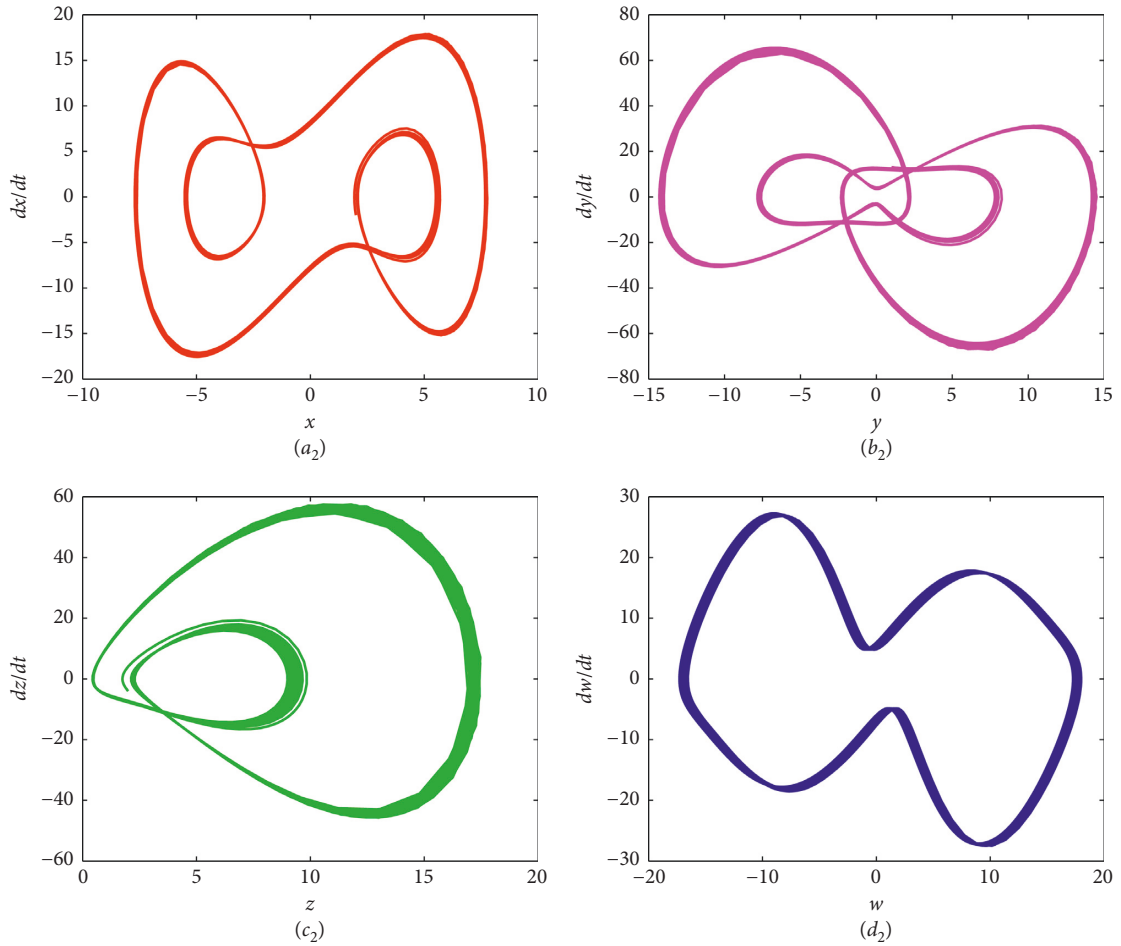

FIGURE 2: Phase diagrams of Experiment 1 with $a = 2, b = 1$, $t = 1000$: (a_2) phase diagram of x; (b_2) phase diagram of y; (c_2) phase diagram of z; (d_2) phase diagram of w.

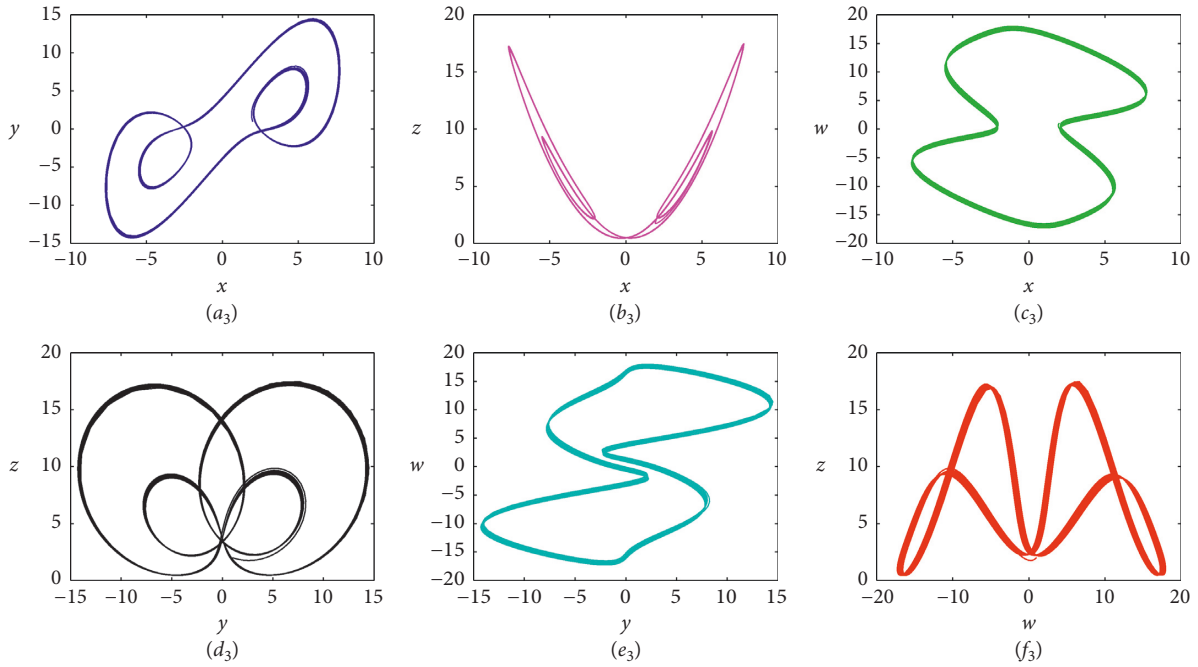

FIGURE 3: Phase portraits of Experiment 1 with $a = 2, b = 1$, $t = 1000$: (a_3) on $x - y$ plane; (b_3) on $x - z$ plane; (c_3) on $x - w$ plane; (d_3) on $y - z$ plane; (e_3) on $y - w$ plane; (f_3) in $z - w$ space.

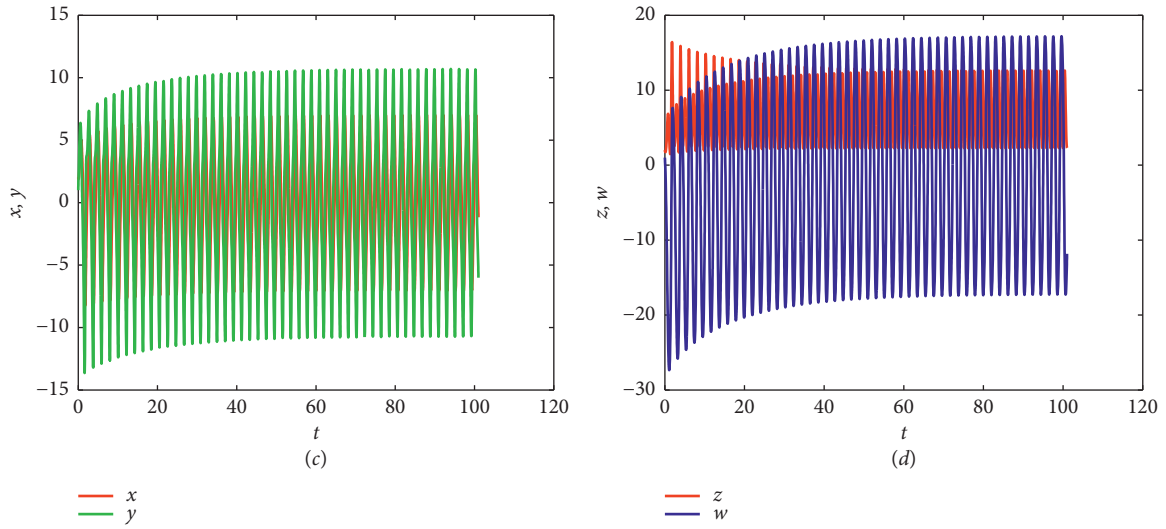

Figure 4: Time evolutions of Experiment 1 with $a = 3$, $b = 5$: (c) x, y states; (d), z, w states.

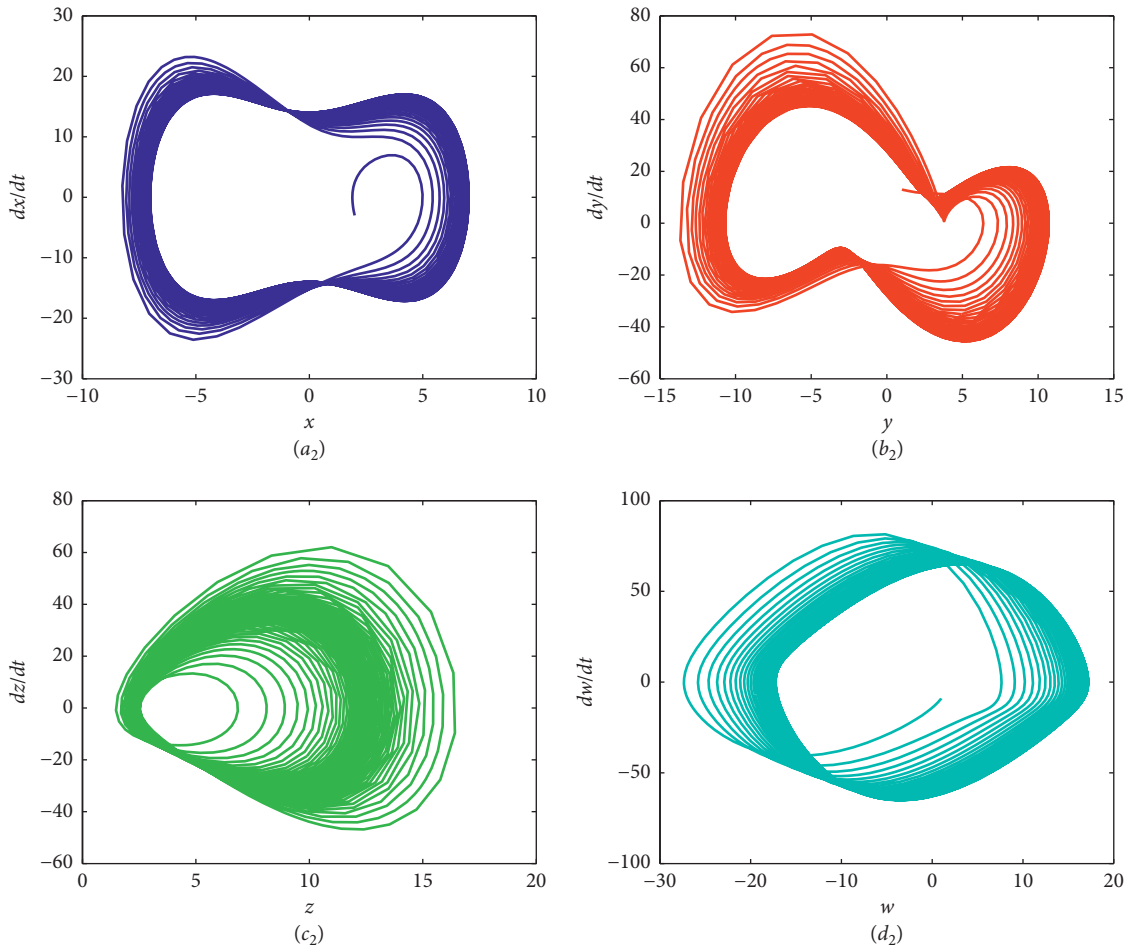

Figure 5: Phase diagrams of Experiment 1 with $a = 3, b = 5$, $t = 100$: (a_2) phase diagram of x; (b_2) phase diagram of y; (c_2) phase diagram of z; (d_2) phase diagram of w.

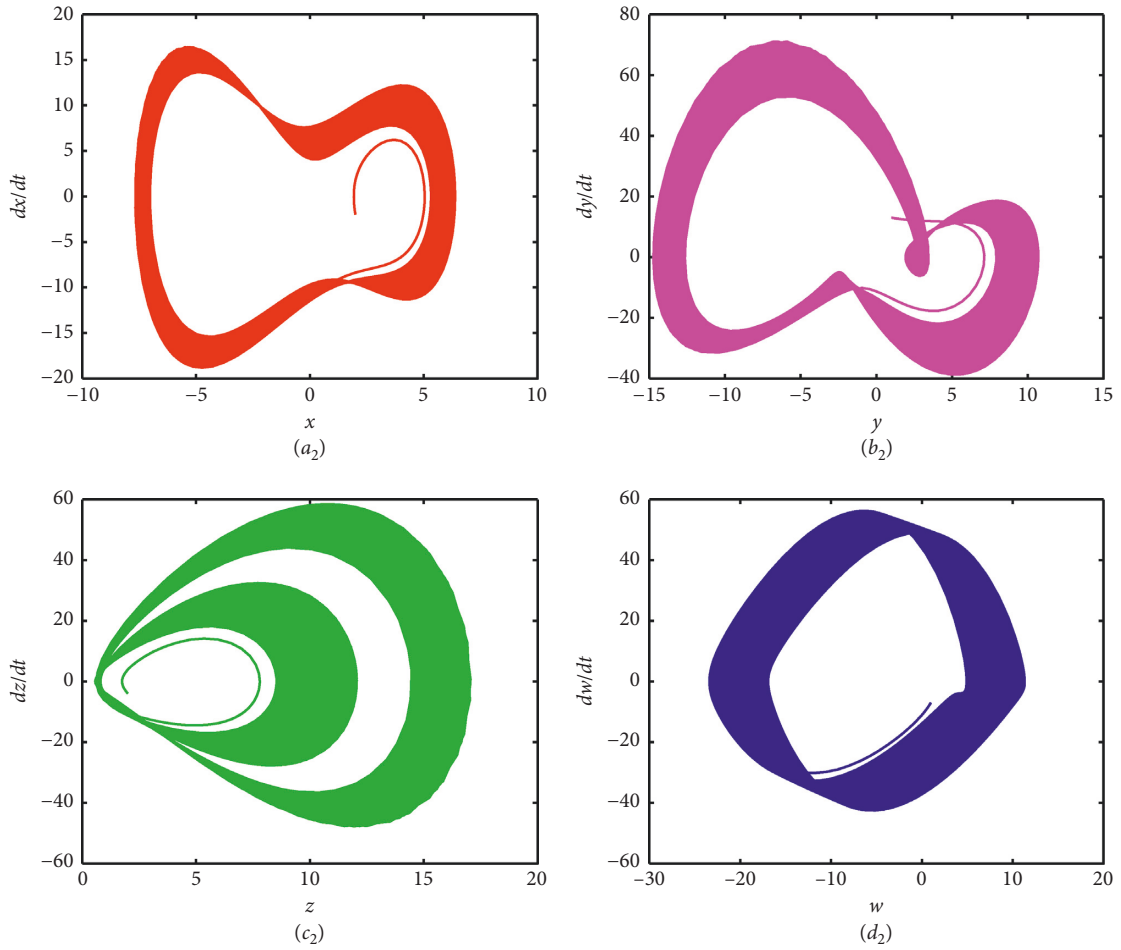

Figure 6: Phase diagrams of Experiment 1 with $a = 2, b = 3, t = 1000$: (a_2) phase diagram of x; (b_2) phase diagram of y; (c_2) phase diagram of z; (d_2) phase diagram of w.

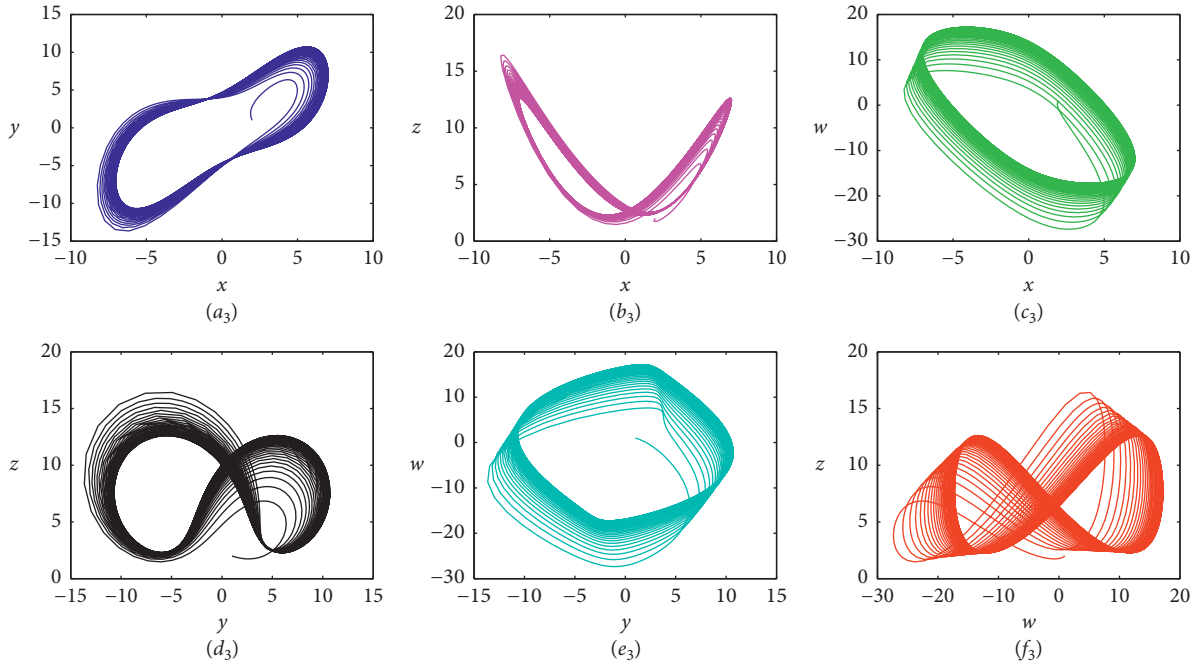

Figure 7: Phase portraits of Experiment 1 with $a = 3, b = 5, t = 100$: (a_3) on $x - y$ plane; (b_3) on $x - z$ plane; (c_3) on $x - w$ plane; (d_3) on $y - z$ plane; (e_3) on $y - w$ plane; (f_3) in $z - w$ space.

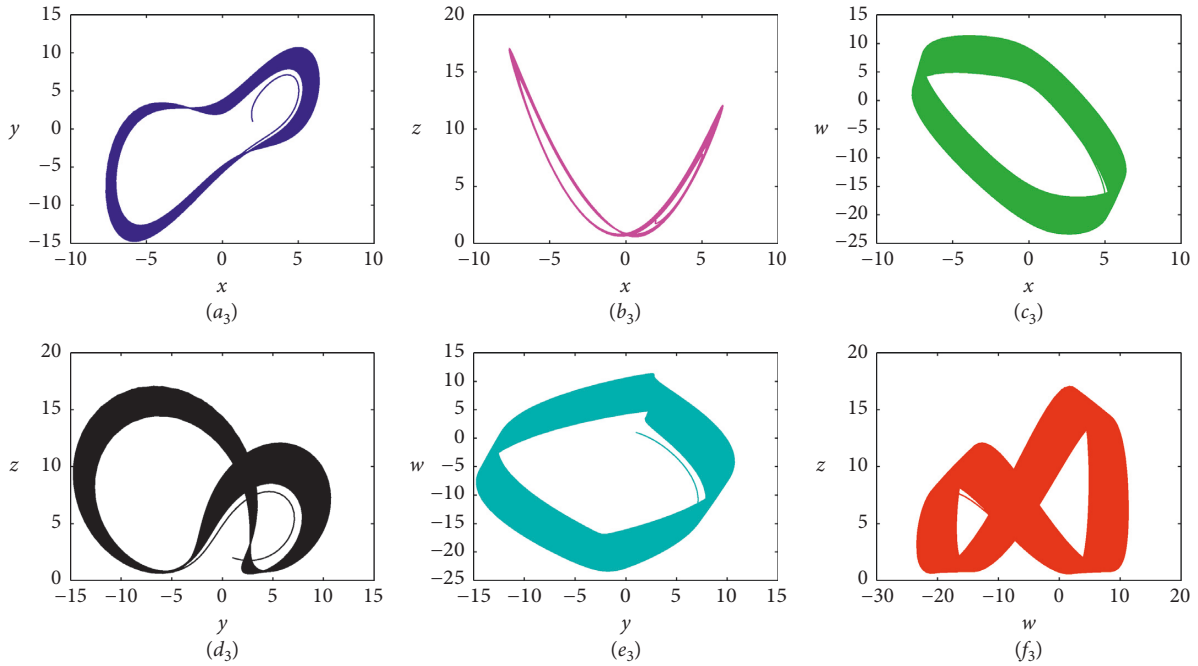

Figure 8: Phase portraits of Experiment 1 with $a = 2, b = 3, t = 1000$: (a_3) on $x - y$ plane; (b_3) on $x - z$ plane; (c_3) on $x - w$ plane; (d_3) on $y - z$ plane; (e_3) on $y - w$ plane; (f_3) in $z - w$ space.

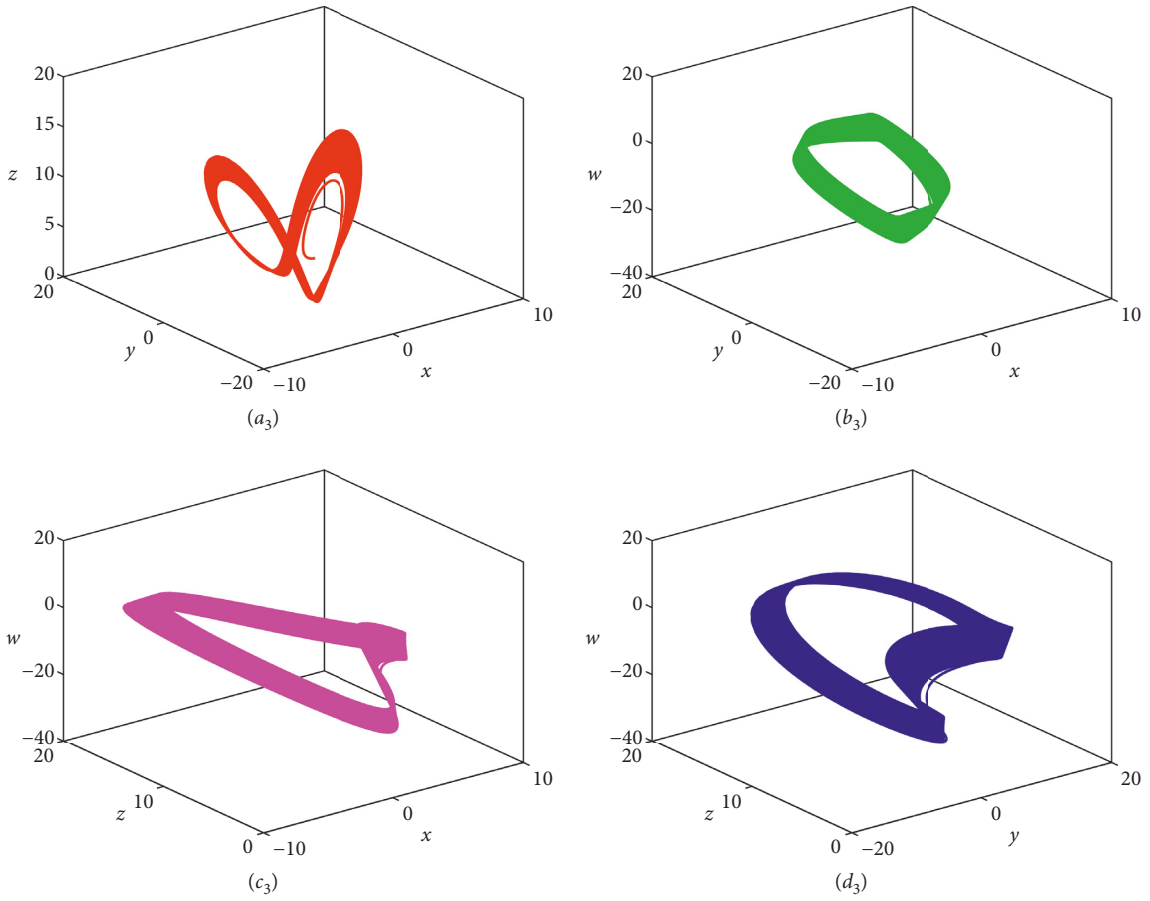

Figure 9: Phase portraits of Experiment 1 with $a = 2, b = 3, t = 1000$: (a_3) on $x - y - z$ plane; (b_3) on $x - y - w$ plane; (c_3) on $x - z - w$ plane; (d_3) on $y - z - w$ plane.

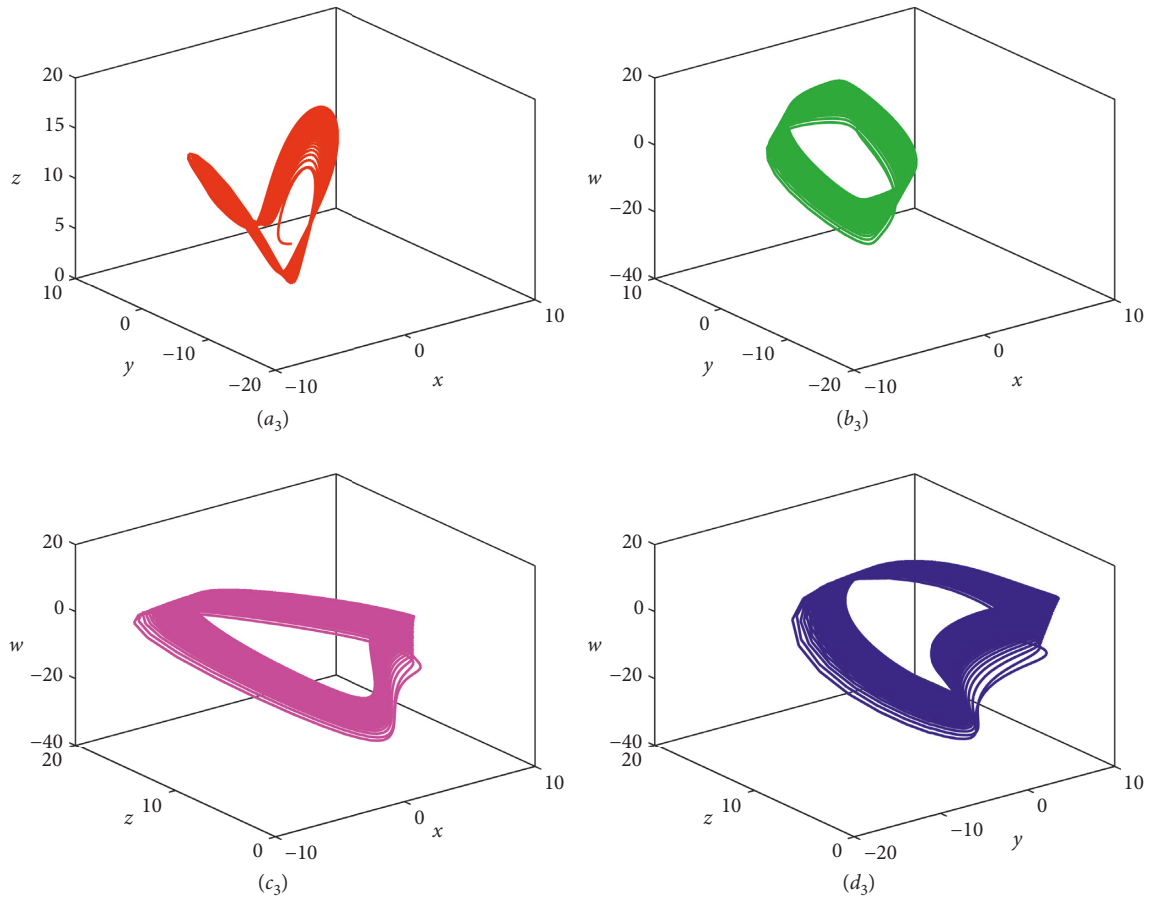

FIGURE 10: Phase portraits of Experiment 1 with $a = 4, b = 5, t = 1000$: (a_3) on $x - y - z$ plane; (b_3) on $x - y - w$ plane; (c_3) on $x - z - w$ plane; (d_3) on $y - z - w$ plane.

Replacing the first line of equation (5) with the initial conditions (6) and solving equation (5) that has been replaced by the initial conditions (6), we can get a numerical solution $x_n(t_j), y_n(t_j), z_n(t_j), w_n(t_j)$ of systems (1) and (2) on $[T_0, T_1]$.

On $[T_1, T_2]$, select the second kind Chebyshev nodes $t_i = (T_2 + T_1/2) - (T_2 - T_1/2)\cos(\pi i/M), i = 0, 1, 2, \ldots, M$ because $x_n(T_1), y_n(T_1), z_n(T_1), w_n(T_1)$ have been obtained on $[T_0, T_1]$. Using (4), we can get

$$\begin{aligned}
\sum_{i=1}^{M} r_i(T_1)x_n(t_i) &= x_n(T_1),\\
\sum_{i=1}^{M} r_i(T_1)y_n(t_i) &= y_n(T_1),\\
\sum_{i=1}^{M} r_i(T_1)z_n(t_i) &= z_n(T_1),\\
\sum_{i=1}^{M} r_i(T_1)w_n(t_i) &= w_n(T_1).
\end{aligned} \tag{7}$$

Replacing the first line of equation (5) with the initial conditions (7) and solving equation (5) that has been replaced by the initial conditions (7), we can get a numerical solution $x_n(t_j), y_n(t_j), z_n(t_j), w_n(t_j)$ of systems (1) and (2) on $[T_1, T_2]$.

Similarly, on $[T_{i-1}, T_i]$, $i = 3, 4, \ldots, N$, we can get the numerical solution of systems (1) and (2) on $[T_{i-1}, T_i]$. After obtaining the numerical solution for all subintervals, these solutions are combined to obtain a numerical solution to equation (1) over the entire interval $[0, T]$.

It is easy to see that the present method provides a globally smooth numerical solution due to the continuity of the numerical solution obtained and its first-order derivative at the common end point of two adjacent intervals.

Based on above formulas, a computer code has been programmed. The existence, uniqueness, and convergence of the approximate solution are ensured by using the computer code.

From above the meshless collocation method, we can get the following theorem.

Theorem 1. *If $\{t_j\}_{j=1}^{\infty}$ is the countable dense point in $[0, T]$, the linear iterative format (3) is the convergence, $x(t), y(t), z(t), w(t)$ is the solution of equation (1), $x_n(t), y_n(t), z_n(t), w_n(t)$ is the solution of equation (3), and $x_n(t_j), y_n(t_j), z_n(t_j), w_n(t_j)$ is the solution of equation (5). Then,*

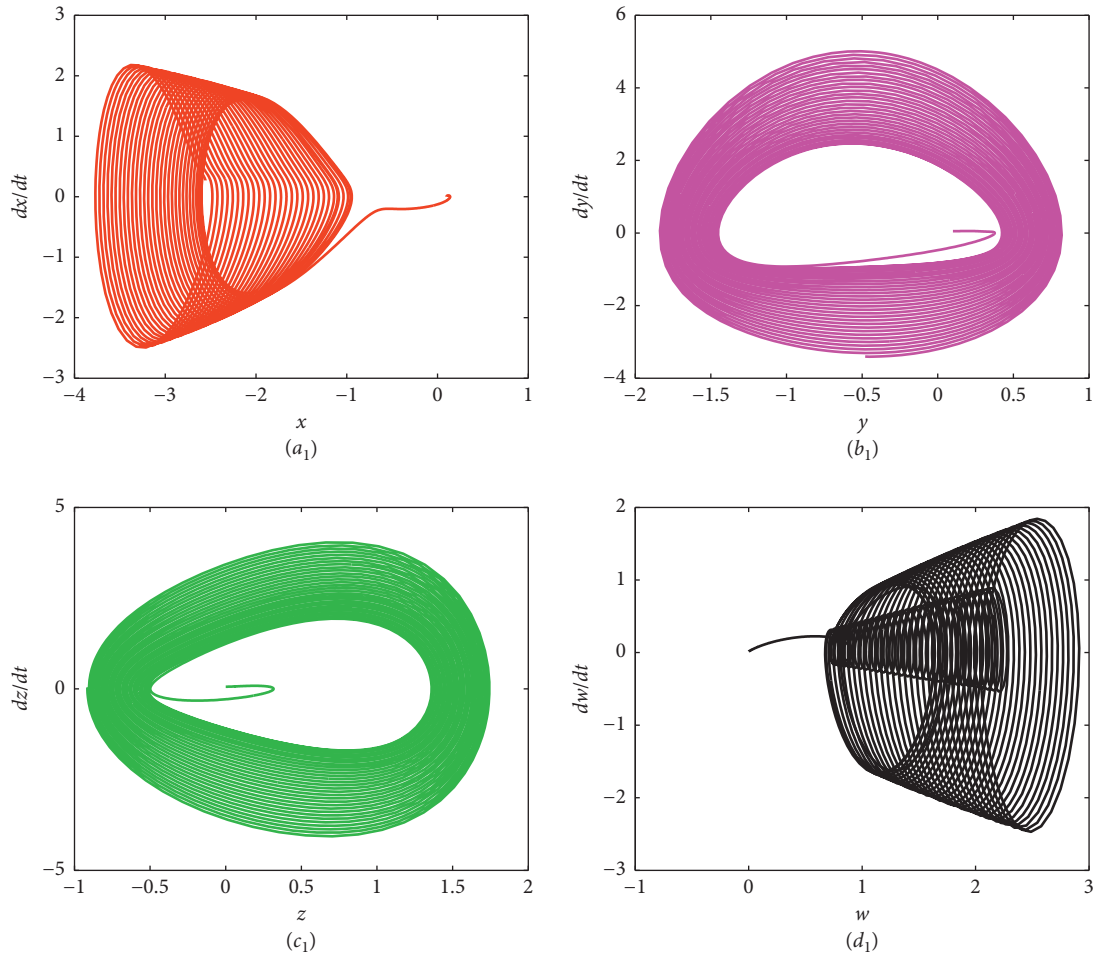

Figure 11: Phase portraits of Experiment 2 with $a = 0.1, t = 100$: (a_1) phase diagram of x; (b_1) phase diagram of y; (c_1) phase diagram of z; (d_1) phase diagram of w.

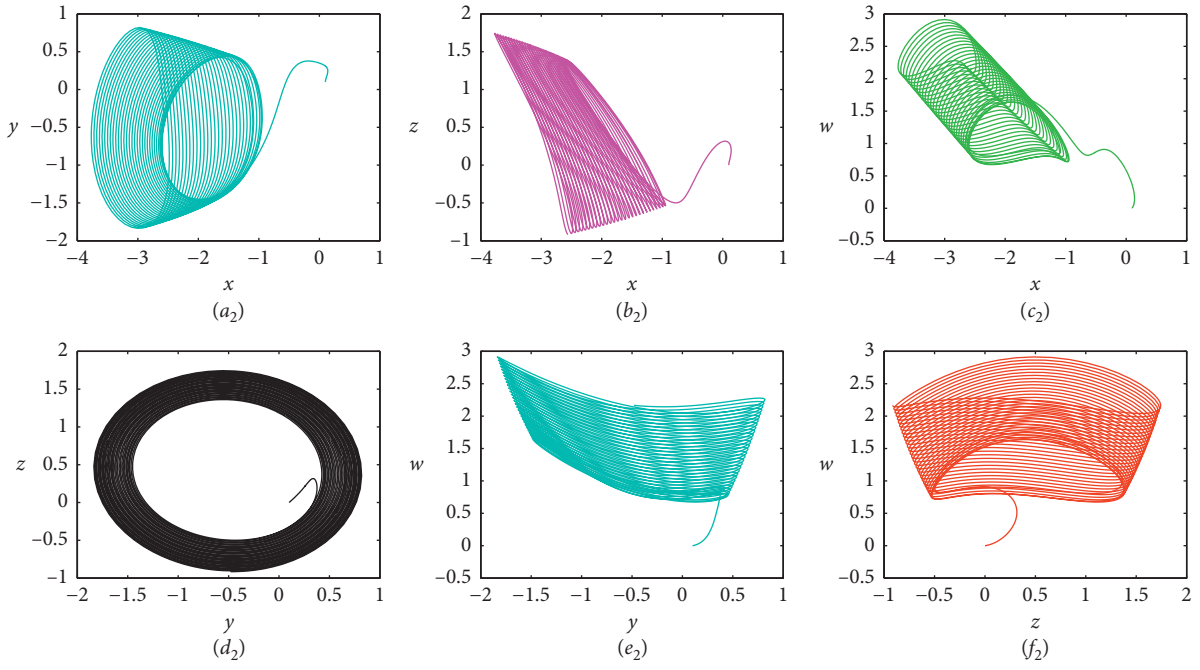

Figure 12: Phase portraits of Experiment 2 with $a = 0.1, t = 100$: (a_2) on $x - y$ plane; (b_2) on $x - z$ plane; (c_2) on $x - w$ plane; (d_2) on $y - z$ plane; (e_2) on $y - w$ plane; (f_2) on $z - w$ plane.

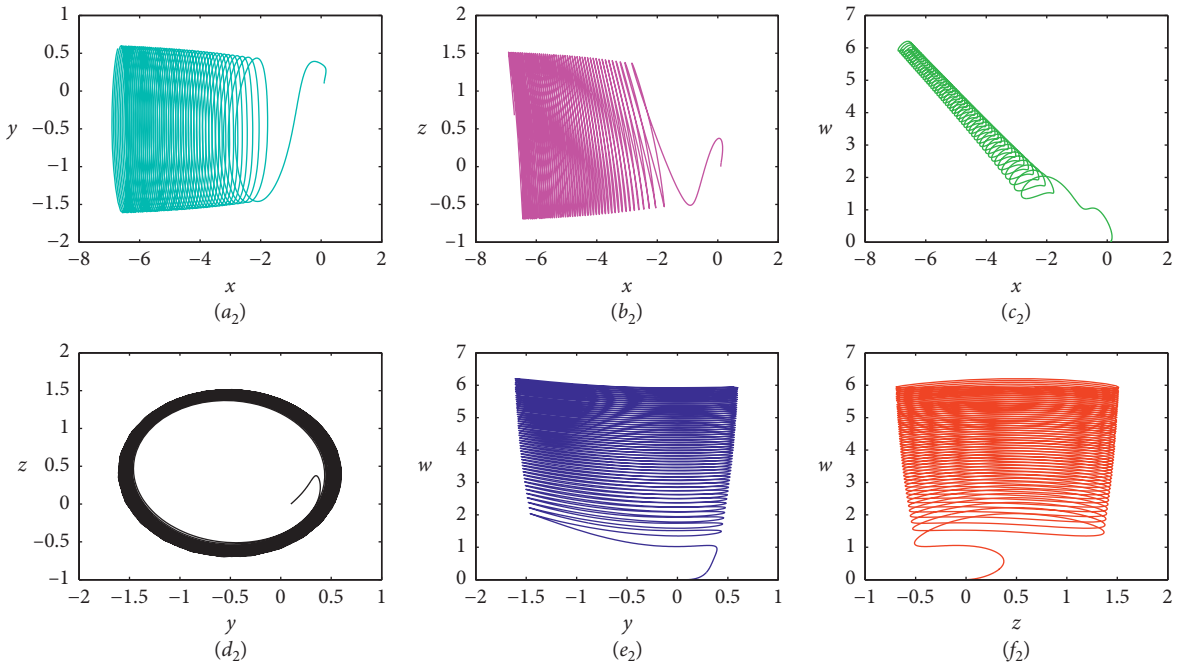

FIGURE 13: Phase portraits of Experiment 2 with $a = 0.01, t = 80$: (a_2) on $x - y$ plane; (b_2) on $x - z$ plane; (c_2) on $x - w$ plane; (d_2) on $y - z$ plane; (e_2) on $y - w$ plane; (f_2) on $z - w$ plane.

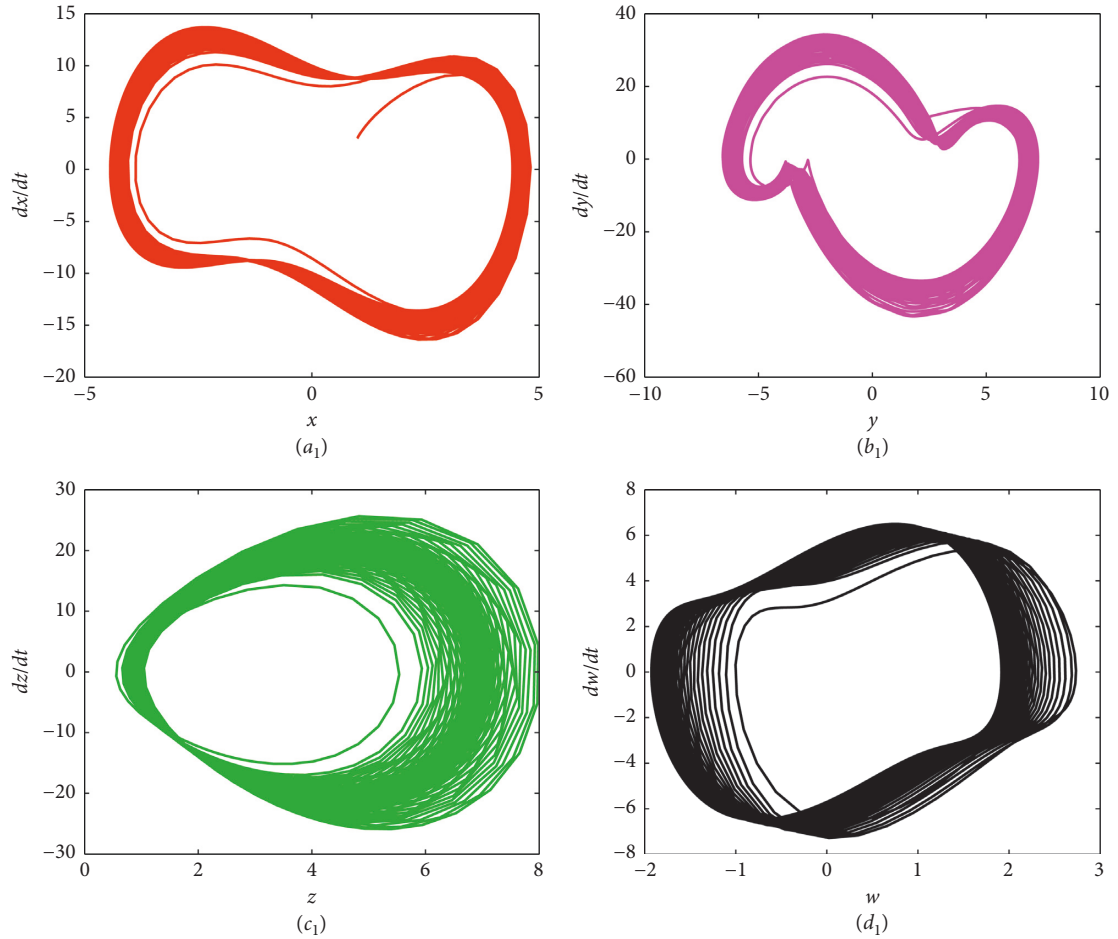

FIGURE 14: Phase portraits of Experiment 3 with $a = 3, t = 3000$: (a_1) phase diagram of x; (b_1) phase diagram of y; (c_1) phase diagram of z; (d_1) phase diagram of w.

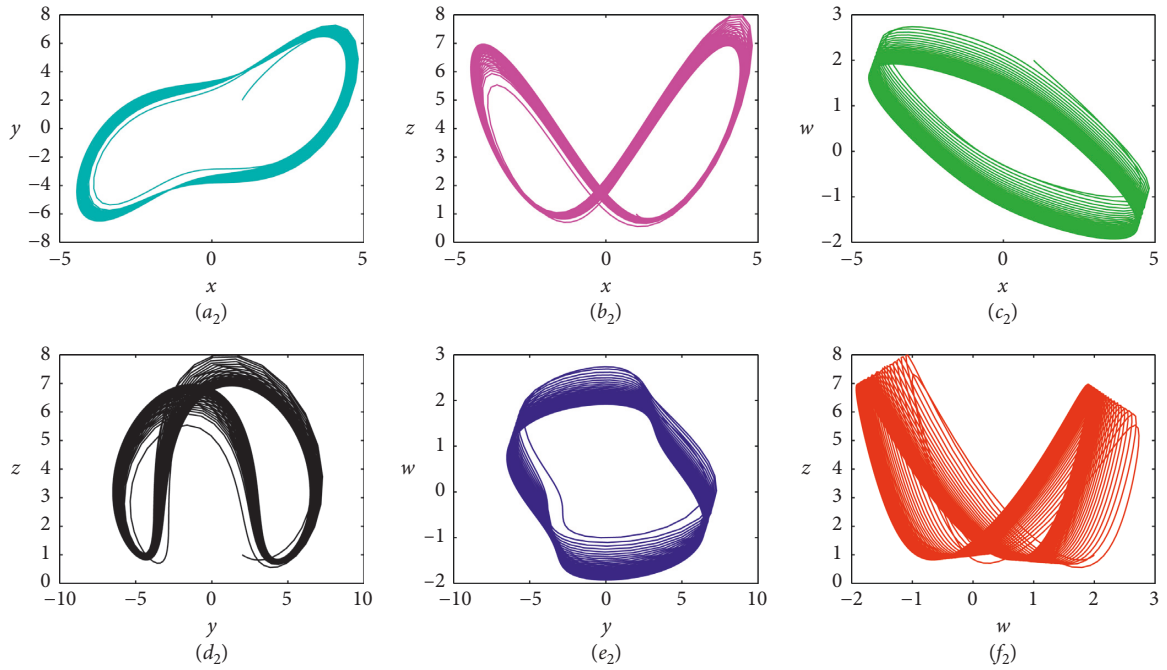

FIGURE 15: Phase portraits of Experiment 3 with $a = 3, t = 3000$: (a_2) on $x - y$ plane; (b_2) on $x - z$ plane; (c_2) on $x - w$ plane; (d_2) on $y - z$ plane; (e_2) on $y - w$ plane; (f_2) on $z - w$ plane.

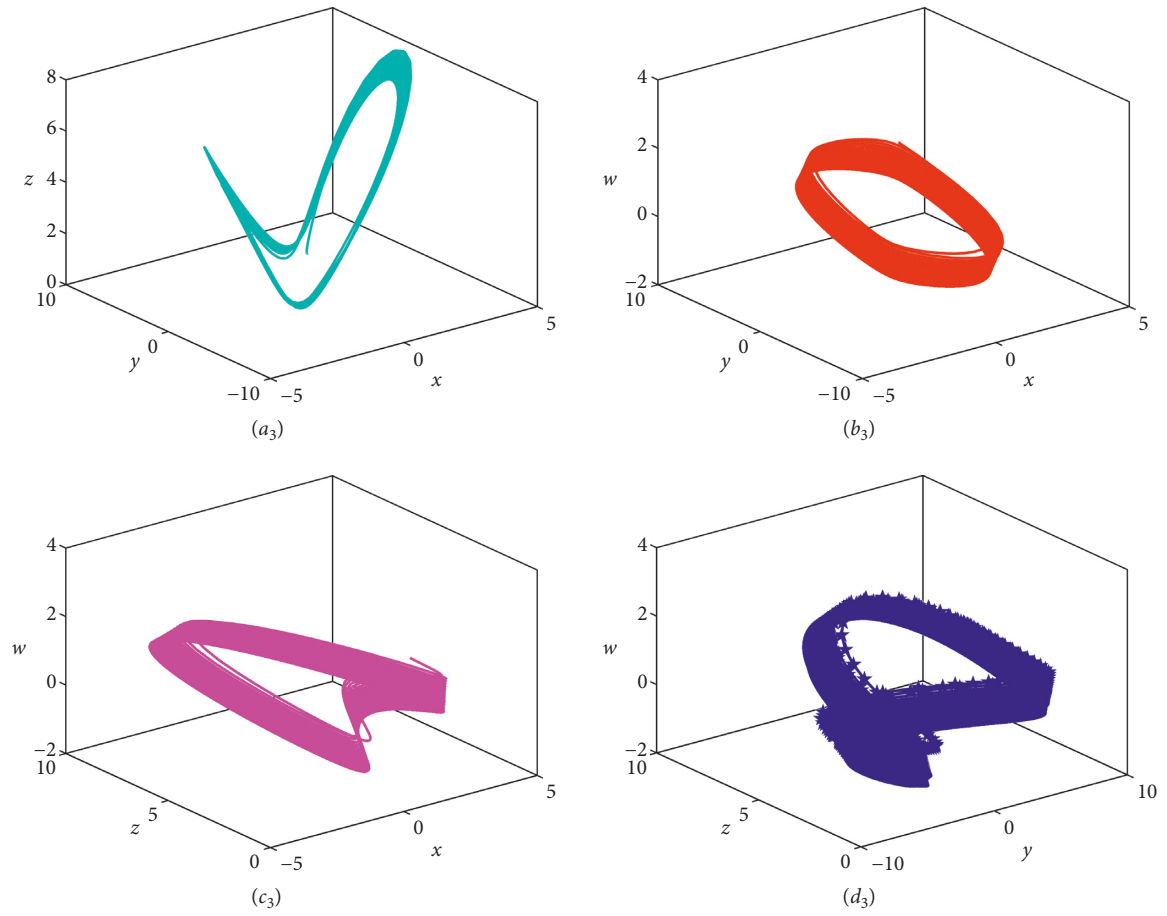

FIGURE 16: Phase portraits of Experiment 3 with $a = 3, t = 3000$: (a_3) in $x - y - z$ space; (b_3) in $x - y - w$ space; (c_3) in $x - z - w$ space; (d_3) in $y - z - w$ space.

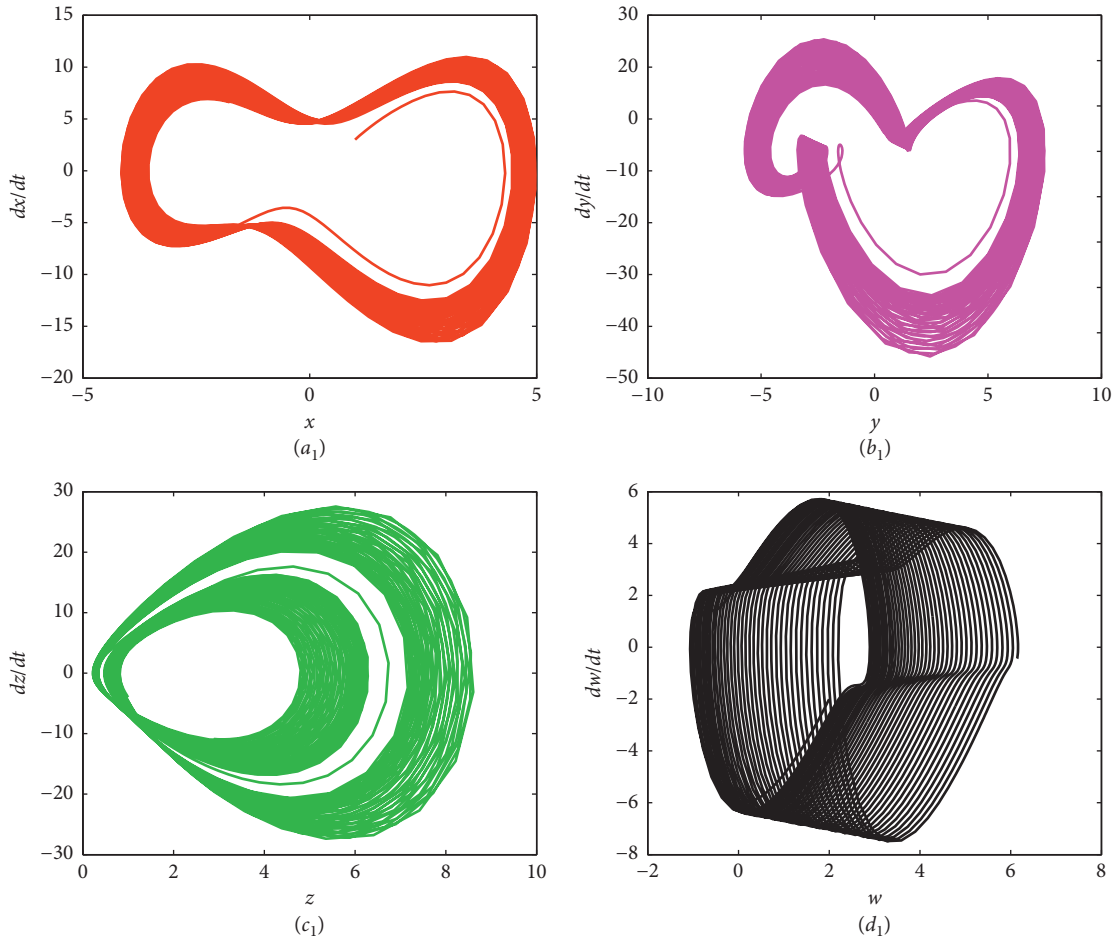

FIGURE 17: Phase portraits of Experiment 3 with $a = 0.1, t = 100$: (a_1) phase diagram of x; (b_1) phase diagram of y; (c_1) phase diagram of z; (d_1) phase diagram of w.

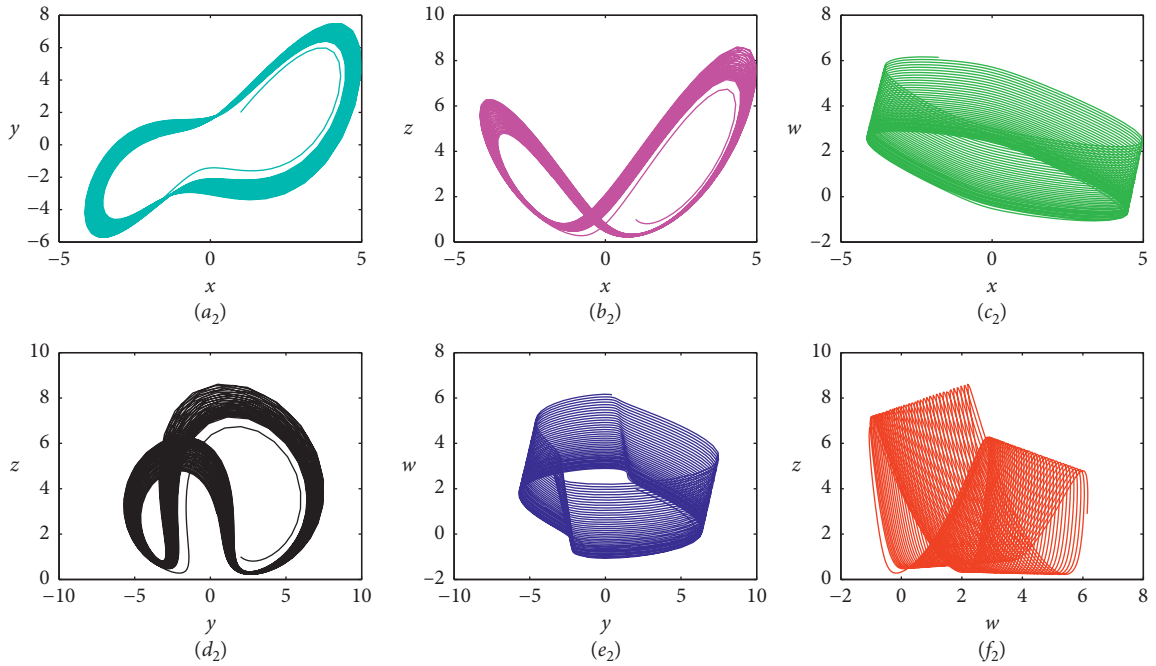

FIGURE 18: Phase portraits of Experiment 3 with $a = 0.1, t = 100$: (a_2) on $x - y$ plane; (b_2) on $x - z$ plane; (c_2) on $x - w$ plane; (d_2) on $y - z$ plane; (e_2) on $y - w$ plane; (f_2) on $w - z$ plane.

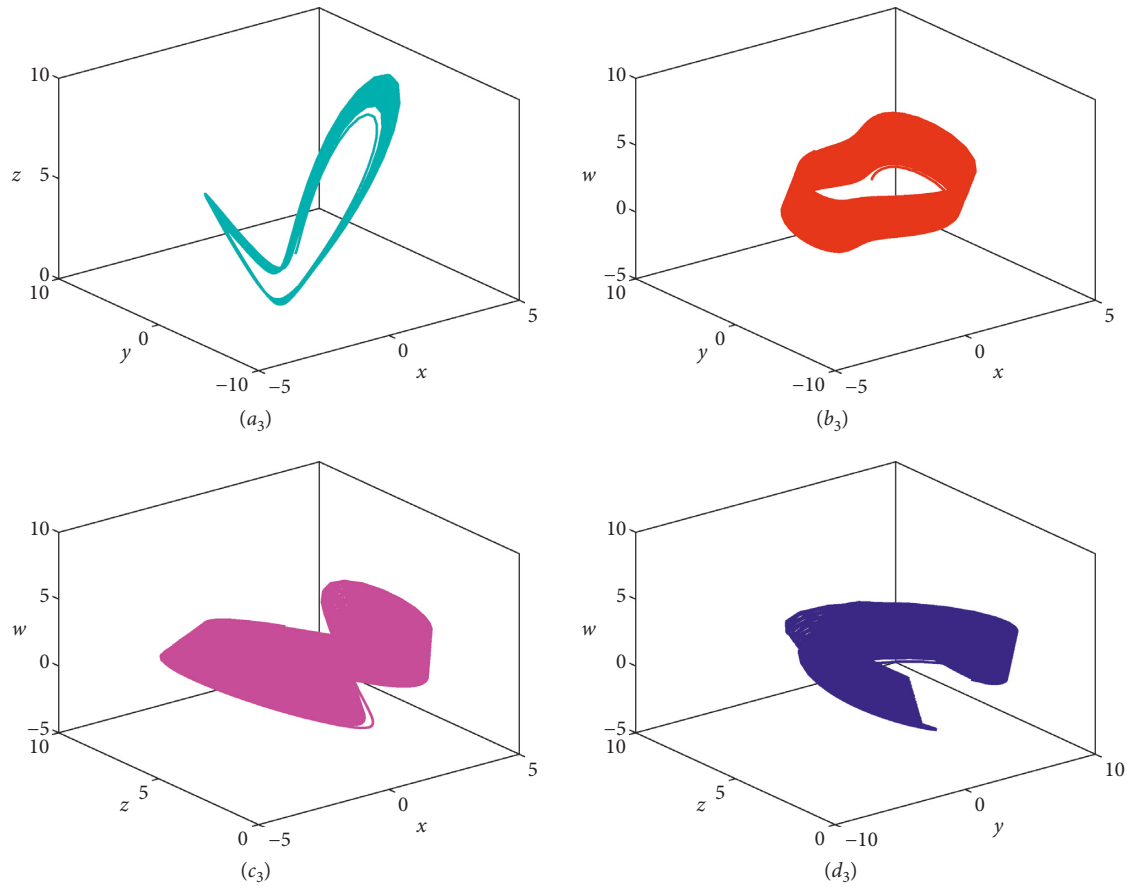

FIGURE 19: Phase portraits of Experiment 3 with $a = 0.1, t = 100$: (a_3) in $x - y - z$ space; (b_3) in $x - y - w$ space; (c_3) in $x - z - w$ space; (d_3) in $y - z - w$ space.

$$\begin{aligned}
\lim_{n\longrightarrow\infty}\left[\lim_{N\longrightarrow\infty} x_n(t_j)\right] &= \lim_{n\longrightarrow\infty} x_n(t) = x(t),\\
\lim_{n\longrightarrow\infty}\left[\lim_{N\longrightarrow\infty} y_n(t_j)\right] &= \lim_{n\longrightarrow\infty} y_n(t) = y(t),\\
\lim_{n\longrightarrow\infty}\left[\lim_{N\longrightarrow\infty} z_n(t_j)\right] &= \lim_{n\longrightarrow\infty} z_n(t) = z(t),\\
\lim_{n\longrightarrow\infty}\left[\lim_{N\longrightarrow\infty} w_n(t_j)\right] &= \lim_{n\longrightarrow\infty} w_n(t) = w(t).
\end{aligned} \tag{8}$$

In numerical experiments, we select the initial iteration value $x_0 = y_0 = z_0 = w_0 = 0; x_1(t_i) = y_1(t_i) = z_1(t_i) = w_1(t_i) = t_i$. *The accuracy of iteration control is* $\varepsilon = 10^{-10}$, *and let* $M = 35, N = T$.

3. Numerical Experiment

In this section, some numerical experiments are studied to demonstrate the accuracy of the present method. The experiments are computed using Matlab R2017a.

Experiment 1. We consider the following four-dimensional system [1]:

$$\begin{bmatrix} \frac{dx}{dt} \\ \frac{dy}{dt} \\ \frac{dz}{dt} \\ \frac{dw}{dt} \end{bmatrix} = \begin{bmatrix} -a & a & 0 & 0 \\ 8 & 0 & 0 & 1 \\ 0 & 0 & -3 & 0 \\ -2 & -b & 0 & 0 \end{bmatrix} \begin{bmatrix} x \\ y \\ z \\ w \end{bmatrix} - \begin{bmatrix} 0 \\ xz \\ -xy \\ 0 \end{bmatrix}, \tag{9}$$

where a and b are the positive parameters of the system, which satisfy the following initial conditions:

$$\begin{aligned}
x(0) &= 2,\\
y(0) &= 1,\\
z(0) &= 2,\\
w(0) &= 1.
\end{aligned} \tag{10}$$

Lyapunov exponents of Experiment 1 are shown in Figure 1. The complex dynamic behaviors of Experiment 1 are shown in Figures 2–9.

Experiment 2. We consider the following four-dimensional system:

$$\begin{bmatrix} \frac{dx}{dt} \\ \frac{dy}{dt} \\ \frac{dz}{dt} \\ \frac{dw}{dt} \end{bmatrix} = \begin{bmatrix} -0.9 & 0.9 & 0 & -0.9 \\ 0.4 & 0.1 & 0 & 0 \\ 0.5 & 0 & -0.1 & 0 \\ a & 0 & 0 & 0 \end{bmatrix} \begin{bmatrix} x \\ y \\ z \\ w \end{bmatrix} + \begin{bmatrix} 0.8yz \\ -xz \\ xy \\ 0.15yz + 0.5y^2 \end{bmatrix}, \tag{11}$$

where a is the real parameter, which satisfies the following initial conditions (Figure 10):

$$\begin{aligned} x(0) &= 0.1, \\ y(0) &= 0.1, \\ z(0) &= 0, \\ w(0) &= 0. \end{aligned} \tag{12}$$

Lyapunov exponents of Experiment 2 are shown in Figure 1. The complex dynamic behaviors of Experiment 2 are shown in Figures 11–13.

Experiment 3. We consider the following four-dimensional system [7]:

$$\begin{bmatrix} \frac{dx}{dt} \\ \frac{dy}{dt} \\ \frac{dz}{dt} \\ \frac{dw}{dt} \end{bmatrix} = \begin{bmatrix} -3 & 3 & 0 & 0 \\ 7 & 0 & 0 & a \\ 0 & 0 & -3 & 0 \\ 0 & -1 & 0 & 0 \end{bmatrix} \begin{bmatrix} x \\ y \\ z \\ w \end{bmatrix} - \begin{bmatrix} 0 \\ 2xz \\ -3x^2 \\ 0 \end{bmatrix}, \tag{13}$$

where a is the parameter of the system, which satisfies the following initial conditions:

$$\begin{aligned} x(0) &= 1, \\ y(0) &= 2, \\ z(0) &= 1, \\ w(0) &= 2. \end{aligned} \tag{14}$$

Lyapunov exponents of Experiment 3 are shown in Figure 1. The complex dynamic behaviors of Experiment 3 are shown in Figures 14–19.

4. Conclusions and Remarks

In this paper, an improved meshless collocation method, which divides the entire intervals $[0, T]$ into N equal subintervals, has been constructed for a class of four-dimensional chaotic or hyperchaotic systems. The numerical results demonstrate that this approach is more effective and accurate than other mesheless collocation methods. Some new complex dynamical behaviors are shown by using the improved method. It is worth noting that the improved method can also be used to solve other similar problems [19, 20]. In the further work, we will be devoted to studying some fractional-order chaotic systems.

Data Availability

The data used to support the findings of this study are available from the corresponding author upon request.

Conflicts of Interest

The authors declare that there are no conflicts of interest regarding the publication of this article.

Acknowledgments

This study was supported by the Natural Science Foundation of Inner Mongolia (2017MS0103), Inner Mongolia Maker Collaborative Innovation Center of Jining Normal University, and National Natural Science Foundation of China (11361037).

References

[1] Q. Yang and Y. Liu, "A hyperchaotic system from a chaotic system with one saddle and two stable node-foci," *Journal of Mathematical Analysis and Applications*, vol. 360, no. 1, pp. 293–306, 2009.

[2] J. P. Singh and B. K. Roy, "Coexistence of asymmetric hidden chaotic attractors in a new simple 4-D chaotic system with curve of equilibria," *Optik*, vol. 145, pp. 209–217, 2017.

[3] S. Bowong and P. V. E. McClintock, "Adaptive synchronization between chaotic dynamical systems of different order," *Physics Letters A*, vol. 358, no. 2, pp. 134–141, 2006.

[4] W. Wu and Z. Chen, "Hopf bifurcation and intermittent transition to hyperchaos in a novel strong four-dimensional hyperchaotic system," *Nonlinear Dynamics*, vol. 60, no. 4, pp. 615–630, 2010.

[5] X.-J. Tong, M. Zhang, Z. Wang, Y. Liu, and J. Ma, "An image encryption scheme based on a new hyperchaotic finance system," *Optik*, vol. 126, no. 20, pp. 2445–2452, 2015.

[6] W. Wu, Z. Chen, and Z. Yuan, "The evolution of a novel four-dimensional autonomous system: among 3-torus, limit cycle, 2-torus, chaos and hyperchaos," *Chaos, Solitons & Fractals*, vol. 39, no. 5, pp. 2340–2356, 2009.

[7] J. P. Singh and B. K. Roy, "The nature of Lyapunov exponents is (+, +, −, −). Is it a hyperchaotic system?," *Chaos, Solitons & Fractals*, vol. 92, pp. 73–85, 2016.

[8] S. Dadras and H. R. Momeni, "Four-scroll hyperchaos and four-scroll chaos evolved from a novel 4D nonlinear smooth autonomous system," *Physics Letters A*, vol. 374, no. 11-12, pp. 1368–1373, 2010.

[9] J.-P. Berrut, "Rational functions for guaranteed and experimentally well-conditioned global interpolation," *Computers & Mathematics with Applications*, vol. 15, no. 1, pp. 1–16, 1988.
[10] J.-P. Berrut and L. N. Trefethen, "Barycentric Lagrange interpolation," *SIAM Review*, vol. 46, no. 3, pp. 501–517, 2004.
[11] C. Schneiaer and W. Werner, "Some new aspects of rational interpolation," *Mathematics of Computation*, vol. 175, pp. 285–299, 1986.
[12] R. Baltensperger and J.-P. Berrut, "The linear rational collocation method," *Journal of Computational and Applied Mathematics*, vol. 134, no. 1-2, pp. 243–258, 2001.
[13] S. P. Li and Z. Q. Wang, *Barycentric Interpolation Collocation Method for Nonlinear Problems*, National Defense Industry Press, Beijing China, 2015.
[14] S. P. Li and Z. Q. Wang, *High-Precision Non-grid Center of Gravity Interpolation Collocation Method: Algorithm, Program and Engineering Application*, Science Press, Beijing China, 2012.
[15] Y. Wang, D. Tian, and Z. Li, "Numerical method for singularly perturbed delay parabolic partial differential equations," *Thermal Science*, vol. 21, no. 4, pp. 1595–1599, 2017.
[16] F. Liu, Y. Wang, and S. Li, "Barycentric interpolation collocation method for solving the coupled viscous Burgers' equations," *International Journal of Computer Mathematics*, vol. 95, no. 11, pp. 2162–2173, 2018.
[17] X. Zhou, J. Li, Y. Wang, and W. Zhang, "Numerical simulation of a class of hyperchaotic system using barycentric Lagrange interpolation collocation method," *Complexity*, vol. 2019, Article ID 1739785, 13 pages, 2019.
[18] M. J. Du, J. M. Li, Y. L. Wang, and W. Zhang, "Numerical simulation of a class of three-dimensional Kolmogorov model with chaotic dynamic behavior by using barycentric interpolation collocation method," *Complexity*, vol. 2019, Article ID 3426974, 14 pages, 2019.
[19] J. Vega, A. Murari, S. González, A. Pereira, and I. Pastor, "Spatial location of local perturbations in plasma emissivity derived from projections using conformal predictors," *Nuclear Instruments and Methods in Physics Research Section A: Accelerators, Spectrometers, Detectors and Associated Equipment*, vol. 720, pp. 14–19, 2013.
[20] A. Murari, N. Bekris, J. Figueiredo et al., "Implementation and exploitation of JET enhancements at different fuel mixtures in preparation for DT operation and next step devices," *Fusion Engineering and Design*, vol. 146, pp. 741–744, 2019.